ACS APPLIED MATERIALS & INTERFACES

Research Article

www.acsami.org

Deposition SnO_2/Nitrogen-Doped Graphene Nanocomposites on the Separator: A New Type of Flexible Electrode for Energy Storage Devices

Junfei Liang,[†,‡] Zhi Cai,[†] Yu Tian,[†] Lidong Li,[†] Jianxin Geng,[‡] and Lin Guo*[,†]

[†]School of Chemistry and Environment, Beihang University, Beijing 100191, P. R. China

[‡]Technical Institute of Physics and Chemistry, Chinese Academy of Sciences, Beijing 100190, P. R. China

ABSTRACT: It is currently very urgent to develop flexible energy storage devices because of the growing academic interest in and strong technical demand of flexible electronics. Exploration of high-performance electrode materials and a corresponding assembly method for fabrication of flexible energy storage devices plays a critical role in fulfilling this demand. Here, we have developed a facile, economic, and green hydrothermal process to synthesize ultrasmall SnO_2 nanocrystallites/nitrogen-doped graphene nanocomposites (USNGs) as a high-performance electrode material for Li-ion batteries (LIBs). Furthermore, using the glass microfiber filters (GMFs) as supporting substrate, the novel flexible USNG−GMF bilayered films have been prepared by depositing the as-prepared USNG on GMF through a simple vacuum filtration. Significantly, for the first time, the flexible USNG−GMF bilayered films have directly been used for assembling LIBs, where the GMF further functions as a separator. The obtained highly robust, binder-free, conducting agent-free, and current collector-free new type of flexible electrodes show excellent LIB performance.

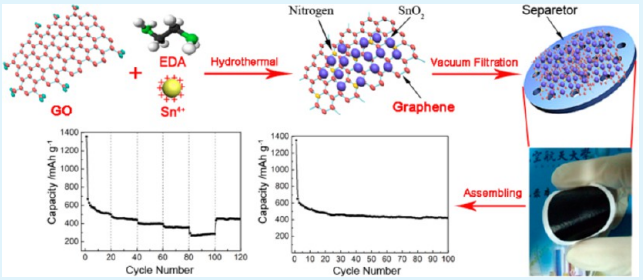

KEYWORDS: *nitrogen-doped graphene, SnO_2, films, flexible electrodes, Li-ion batteries*

1. INTRODUCTION

It is currently very urgent to develop flexible or bendable energy storage devices because of the growing academic interest in and strong technical demand of flexible electronics such as rollup displays, stretchable integrated circuits, and wearable devices.[1,2] Owing to their attractive characters, including high gravimetric and volumetric energy densities, high voltage, and long cycle life, Li-ion batteries (LIBs) not only are widely used in conventional electronic devices[3,4] but also hold great promise for powering flexible electronics if they can be fabricated into the flexible form.[5] However, the large-scale use of flexible LIBs is limited mainly by the low capability of fabricating flexible electrodes with robust mechanical property and high Li storage performance.[6−8] One strategy to solve this problem is the approach that includes mixing the electrode materials with conductive agents and polymer binders and then coating the mixture on a flexible substrate. However, this strategy suffers from the time-consuming and complicated preparation process, as well as the instability of the most flexible substrates during the electrode preparation process.[9] Besides, it is worth noting that the binders and the substrates make no contribution to the Li storage capacity, and the conductive agent exhibits poor Li storage performance. Thus, these components significantly decrease the energy density of flexible LIBs. From the perspective of obtaining optimal performance, the optimization of the electrode system can increase the energy density of LIBs. In particular, binder-free, conducting agent-free, and current collector-free construction can effectively fulfill this demand.[10] The large-scale use of flexible LIBs is also limited by another factor: lack of reliable electrode materials that combine superior electronic conductivity, high mechanical flexibility, high electrochemical stability, and excellent LIB performance.[11] Therefore, it urgently needs to explore the high-performance materials as well as develop the corresponding efficient assembly methods for fabrication of flexible LIBs.

Graphene, a two-dimensional closely packed and single-atom thick honeycomb carbon lattice, shows a lot of intriguing properties such as superior electronic conductivity,[12] high mechanical strength and elasticity,[13] electrochemical stability, and so on.[14,15] Additionally, it has been recently reported that graphene nanosheets can be simply synthesized in large quantity by chemical transformation from inexpensive and commercially available graphite,[16] and by a simple vacuum filtration of the colloidal dispersion of graphene nanosheets, a flexible graphene film can be easily obtained through a flow-directed assembly process.[17−19] Particularly, compared with other film-like carbonaceous material, such as graphite foil or carbon nanotube (CNT) film, the free-standing graphene film exhibited better mechanical strength and stiffness.[11] Thus, we

Received: September 18, 2013
Accepted: November 5, 2013
Published: November 5, 2013

expect that the graphene film may be a reliable material for the flexible energy storage devices. However, when used as anode materials for LIBs, the Li storage capacity of the graphene films is very low (only around 100 mAh g^{-1}), although they exhibit good cycle performance.[20] This results indicate that the graphene films themselves are unsuitable for application as flexible anode materials for LIBs. Incorporation of an electrode material with higher Li storage capacity into the graphene films and doping of heteroatoms into the graphene lattice are two practical ways to enhance the Li storage capacity of the graphene films.[11,21] Recently, some free-standing graphene nanocomposite thin films have been fabricated, and the as-prepared films show potential application for flexible LIBs.[22−24] However, as far as we know, the previously reported flexible graphene nanocomposite film electrodes without a supporting substrate exhibited poor mechanical strength, which seriously restricts their applications in flexible LIBs.

Transition metal oxides (MO_x, M: Sn, Fe, Co, Cu, etc.), which show advantages in high theoretical capacity (>600 mAh g^{-1}), low cost, and environmentally friendly synthesis processes, have been developed as electrode materials for LIBs since the 1980s.[25] They could be used as ideal hybrid electrode materials for improving the capacity of the graphene films. Due to its low discharge potential and high theoretical Li storage capacity, SnO_2 has attracted more attention than other MO_x.[26] However, the practical applications of the MO_x as anode materials are seriously hindered by their poor cycle and rate performance due to serious volume expansion/contraction during the lithiation/delithiation processes.[27] To develop a high-performance MO_x anode material, various methods have been tested. Compositing MO_x with carbon materials is an effective strategy to obtain better Li storage performance by improving the kinetics of charge transfer, increasing the interfacial contact area between the electrolyte and electrode, and effectively accommodating the strain of volume change during the insertion/extraction processes of Li^+. In particular, graphene has attracted great interest in compositing with MO_x for applications as anode materials because of its excellent properties mentioned above.[28] In addition, recent research showed that the Li storage properties of graphene could be obviously improved by doping of nitrogen atoms into the graphene lattice. The special two-dimensional structure of nitrogen-doped (N-doped) graphene with heteroatomic defects and disordered surface morphology shows better electrolyte wettability, increased sheet distance, improved electrical conductivity, and thermal stability. All these factors can facilitate rapid surface Li^+ absorption and ultrafast electron transport and Li^+ diffusion, and thus, the N-doped graphene outperforms the pristine chemically derived graphene and other carbonaceous materials.[21,29] Therefore, we expect that the SnO_2/N-doped graphene nanocomposites may be an excellent electrode material for the flexible LIBs. However, to our best knowledge, the report in this field is rare, and the rarely reported processes for preparing SnO_2/N-doped graphene nanocomposites were complicated.[30,31] Recently, Wang and coworkers developed a new method to prepare SnO_2/N-doped graphene nanocomposites.[31] However, this method involved several steps and usage of a toxic reducing agent (hydrazine monohydrate) in the preparation process, making this approach restricted for application. Moreover, most reported approaches to prepare the N-doped graphene require rigorous conditions, special instruments, and toxic nitrogen-containing precursors (usually NH_3 or pyridine). Furthermore, previous reports indicated the the LIB performance of the MO_x/graphene composites is highly dependent on the size and dispersion state of MO_x nanoparticles. The small particle size with the addition of good dispersion state can endow the composite electrode materials high Li storage capacity and good rate performance.[32] However, until now, most MO_x nanocrystallites in the reported MO_x/graphene composites have relatively bigger sizes (from 10 nm to hundreds of nanometers) with poor dispersion state.[33] Therefore, it is a challenge to explore facile, economic, and eco-friendly methods for synthesis of small sized MO_x nanocrystallites/N-doped graphene nanocomposites.

In this study, we developed a novel approach for preparing a flexible anode for LIBs. This method has the following advantages: (i) A facile, economic, and green one-step hydrothermal procedure to chemically synthetize ultrasmall SnO_2 nanocrystallites/nitrogen-doped graphene nanocomposites (USNGs) from graphene oxide (GO) dispersion, ethylenediamine (EDA), and Sn^{4+} was developed for the first time. This synthesis method may provide an effective approach for the synthesis of other ultrasmall MO_x nanocrystallites/N-doped graphene nanocomposites for different applications. (ii) A novel flexible USNG−GMF bilayered film has been explored by depositing the as-prepared USNG on glass microfiber filters (GMFs) through a simple vacuum filtration. Significantly, for the first time, the bilayered film has directly been used for assembling LIBs, where the GMF functions as a separator and supporting substrate. The obtained highly robust, binder-free, conducting agent-free, and current collector-free new type of flexible electrodes show excellent LIB performance. Our new approach for the fabrication of flexible USNG−GMF bilayered film electrodes can be applied to various other electrode materials, which may be useful in flexible or bendable energy storage devices.

2. EXPERIMENTAL SECTION

2.1. Materials. Graphite powder (325 mesh, with purity >99.99%) was obtained from Alfa Aesar. All other chemicals (purchased from Aladdin-Reagent Inc.) used in this experiment were analytical grade and were used without further purification.

2.2. Preparation of USNG−GMF Bilayered Film. Graphite oxide was prepared from graphite powder according to the modified Hummer's method.[34] To completely remove residual acids and metal ions, the graphite oxide dispersion was subjected to dialysis for 7 days. Afterwards, the GO nanosheet dispersion was obtained by ultrasonic treatment of the above resulting graphite oxide dispersion for 2 h with a frequency of 40 kHz (KH-500, Kunshan, Hechuang Ultrasonic Cleaner Inc). To remove any remaining undispersed solid and obtain the homogeneous GO dispersion, the dispersion of GO nanosheets after ultrasonic treatment was centrifuged for 30 min with a high centrifugal speed of 4000 rpm. Finally, a brown homogeneous dispersion of GO was obtained.

In a typical synthesis of the USNG, 0.5 g of $SnCl_4{\cdot}5H_2O$ was added into a 40 mL suspension of GO with the concentration of 1 mg mL^{-1}. The mixture was sonicated for 5 min before adding 0.5 mL of EDA. Then the mixture was stirred at ambient conditions for 5 min. The resulting solution was transferred to a Teflon-lined stainless steel autoclave of 45 mL volume and kept at 180 °C for 24 h. At last, the as-prepared USNGs were collected by centrifugation and washed several times with deionized water. After that, the as-prepared USNGs were deposited on the Whatman glass microfiber filter (GE Whatman GF/A, diameter 47 mm, pore size 1.6 μm, thickness 260 μm) to form the flexible USNG−GMF bilayered film by the simple vacuum filtration method and then dried at room temperature under vacuum conditions for further characterization and electrochemical measurements.

2.3. Characterizations. X-ray powder diffraction (XRD) analyses were carried out on an X-ray diffractometer (Rigaku Dmax 2200). A

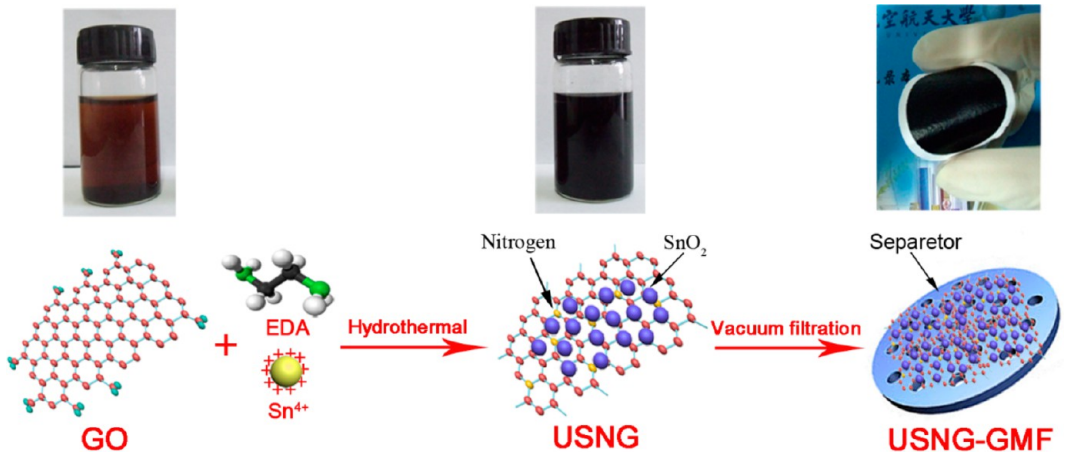

Figure 1. Schematic illustration for the preparation of flexible USNG−GMF.

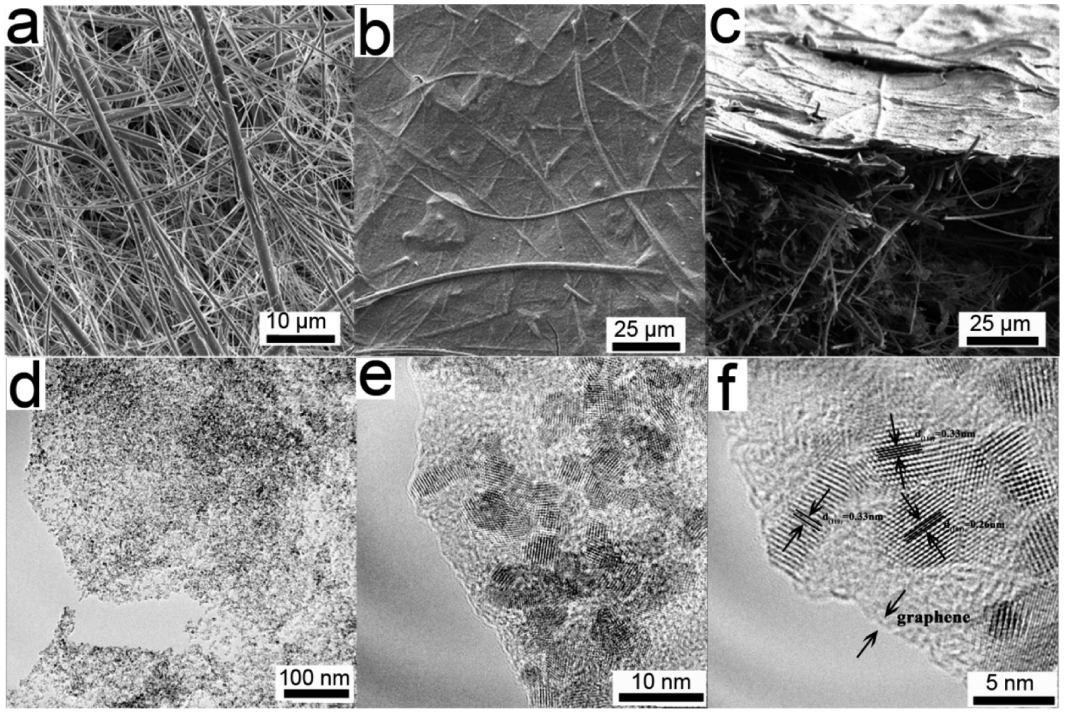

Figure 2. (a,b) Top-view FESEM image of the separator and flexible USNG−GMF; (c) the cross-section images FESEM of the flexible USNG−GMF; (d) TEM; and (e,f) HRTEM image of the USNG nanocomposites.

JEM-2100F transmission electron microscope (JEOL Ltd., Japan) was used for getting the transmission electron microscopy (TEM) and high-resolution TEM (HRTEM) images of the samples. Raman spectra were carried out on a LabRAM HR800 laser Raman spectrometer (HORIBA JobinYvon Co. Ltd., France) using a laser with the wavelength of 488.5 nm. The XPS data were taken on an AXIS Ultra instrument from Kratos Analytical. The IR spectra were carried out through a Nicolet iN10 MX (Thermo Scientific) in the domain 600−4000 cm^{-1}.

2.4. Electrochemical Performance Measurements. The electrochemical performance of the flexible USNG−GMF and the single SnO_2 nanoparticle electrode materials was evaluated as follows: First, USNG−GMF was cut into appropriate sizes, and the cells were designed without using additional conducting agent, polymer binders, separator, and current collectors. In the control experiment, the SnO_2 nanoparticle electrodes were prepared by mixing SnO_2 nanoparticles with carbon black as conducting agent and polyvinylidene fluoride (PVDF) as polymer binder with a mixing ratio of 80%:10%:10% dissolved in *N*-methyl-2-pyrrolidone (NMP) to form the slurry, which was later covered onto a copper foil as current collectors, dried for 10 h under the temperature of 80 °C, punched into small disks with a diameter of 14 mm, and finally compressed under the pressure of 10 MPa. Subsequently, CR2032-type coin cells were fabricated in a highly pure argon-filled glovebox by using the SnO_2 nanoparticles or flexible USNG−GMF as test electrodes and the metallic lithium as counter/reference electrode. Charge−discharge measurements were carried out galvanostatically by using a battery test system (LAND CT2001A model, Wuhan Jinnuo Electronics. Ltd., China) under different current density (100−3000 mA g^{-1}) in the voltage range of 0.005~1.5 V.

3. RESULTS AND DISCUSSION

The flexible USNG−GMF bilayered films were fabricated via a two-step route (Figure 1). In the first step, the USNG was prepared by a hydrothermal process by using $SnCl_4{\cdot}5H_2O$ and GO as precursors and EDA as both a nitrogen source and ligand. In this process, GO was thermally reduced into graphene and doped with nitrogen, and SnO_2 nanocrystallites

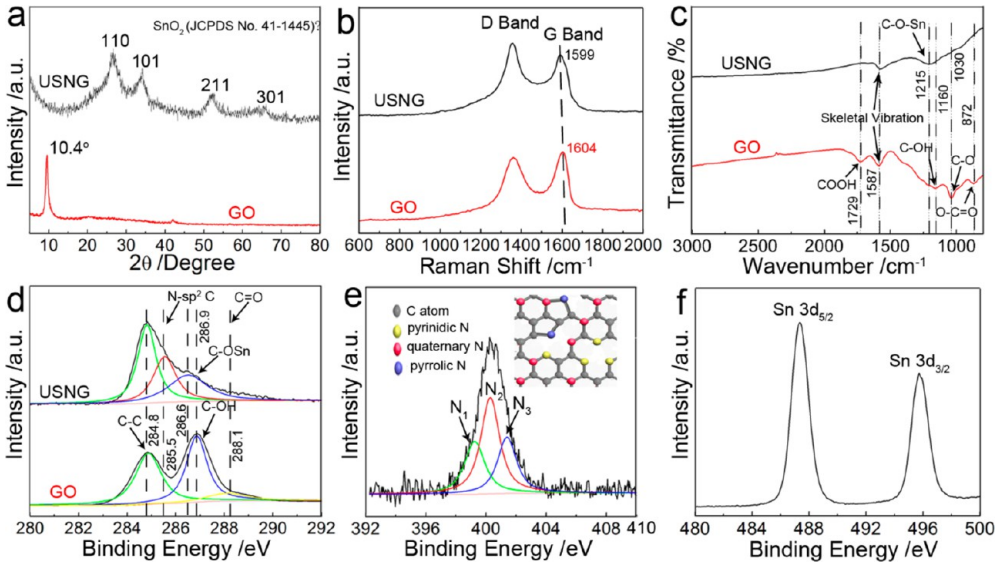

Figure 3. (a) XRD patterns of GO and USNG–GMF paper; (b,c) the Raman and IR spectra of GO and USNG; (d) the high-resolution XPS spectra of the C 1s region for GO and USNG; (e) the high-resolution XPS spectra of the N 1s region for USNG; and (f) Sn 3d XPS spectrum of the USNG.

were in situ formed and uniformly deposited on graphene sheets. Previous studies indicated that GO nanosheets carry epoxy and hydroxyl groups on their basal planes and carboxyl groups at the edge areas.[35] The GO nanosheets were readily dispersed in H_2O to form a uniform suspension with the aid of sonication because of the oxygen-containing species. Upon addition of a $SnCl_4{\cdot}5H_2O$ solution into a GO suspension, Sn^{4+} could be selectively bonded with the oxygen-containing groups through electrostatic force. Hydrolysis reaction between Sn^{4+} ions and OH^- leads to the formation of SnO_2. It is known that EDA is a strong chelating agent that can readily coordinate with Sn^{4+}. Upon addition of EDA into the precursor mixture, complex $Sn_n(EDA)_m^{4+}$ is immediately formed, leading to decreased reactivity between Sn^{4+} and OH^- and formation of ultrasmall SnO_2 nanocrystallites. Meanwhile, the EDA also leads to N-doping of the graphene sheets as the GO is reduced into graphene under the hydrothermal conditions. After the hydrothermal reaction, the color of the solution changes from brown to black, which confirms the successful reduction of GO to graphene. In the second step, the as-prepared USNG was deposited on the GMF filter membrane by a simple vacuum filtration. The USNG–GMF bilayered films are flexible. Compared with the freestanding graphene nanocomposite films, the USNG–GMF films exhibit higher mechanical strength because of the presence of GMF as a supporting substrate in the bilayered films.

A GMF filter membrane is made of randomly oriented glass microfibers (Figure 2a). In contrast, the glass microfibers are uniformly and intimately covered by the USNG in the USNG–GMF bilayered films, as revealed by the top view and cross-section SEM image (Figure 2b, c). Figure 2d displays a TEM image of the USNG at a lower magnification. It is seen that SnO_2 nanocrystallites are uniformly dispersed on the graphene sheet's surface. The average size of the SnO_2 nanocrystallites is smaller than 5 nm, as revealed by the HRTEM image of the USNG (Figure 2e). The lattice-resolved HRTEM image of SnO_2 nanocrystallites exhibits lattice spacing of 0.26 and 0.33 nm, which is corresponding to the d-spacing of (101) and (110) crystal planes of SnO_2, respectively. The strips marked with arrows in Figure 2f show the exiting of graphene nanosheets in the composites. The in situ uniform deposition of the ultrasmall SnO_2 nanocrystallites on graphene sheets can be attributed to the existence of GO and EDA in the reaction system. The abundant existence of oxygen-containing functional groups (epoxide, hydroxyl, and carboxylic acid groups), uniformly distributed on the surface of the GO sheets, can act as anchoring sites for Sn^{4+} through electrostatic attraction.[36] Thereafter, these oxygen-containing groups further act as nucleation centers for the growth of the SnO_2 nanocrystallites. Thus, these oxygen-containing functional-group-assisted nucleation and growth processes ensure the in situ uniform deposition of the SnO_2 nanocrystallites on graphene sheets. In addition to that, the N incorporated in the graphene sheets can also function as nucleation sites, facilitating the morphology and particle size control of the SnO_2 nanocrystallites. Moreover, recent research demonstrated that GO played an important role in the morphology and size of the resultant particles in the composites during the particle growth process due to its surfactant effect. Uniform and small size particles can be obtained from the GO involved systems.[37] In our work, the formation of SnO_2 can be attributed to the hydrolysis reaction of Sn^{4+}. In this process, EDA can function as a legend to control the morphology of the SnO_2 nanocrystallites. Complex $Sn_n(EDA)_m^{4+}$ was formed due to the strong coordination between Sn^{4+} and EDA, as EDA was added into the reaction mixture. The formation of the complex $Sn_n(EDA)_m^{4+}$ decreased the hydrolysis reactivity of Sn^{4+}, thereafter resulting in formation of ultrasmall SnO_2 nanocrystallites. It is noteworthy that the LIB performance of the MO_x/graphene composites is highly dependent on the size and dispersion state of MO_x nanoparticles. The small particle size with the addition of good dispersion state can not only endow the composite electrode materials a superior high surface area to buffer the serious volume expansion/contraction of the MO_x during the charge/discharge processes but also shorten the diffusion distance for Li^+ and bring the satisfied conductivity to single MO_x nanoparticles, which are beneficial for improving capacity and rate performance of MO_x/graphene composite anode materials.[33] The USNG synthesized by our method has the potential

to improve the performance of LIBs due to the existence of the ultrasmall SnO_2 nanocrystallites.

Figure 3a shows the XRD pattern of GO and USNG. GO gives an XRD pattern containing a diffraction peak at 10.4° corresponding to the interlayer spacing of 0.85 nm. For samples of USNG, the diffraction peaks of layered GO disappear, which indicate the successful reduction of GO. No diffraction peak (002) of graphite around 26.6° is observed in the XRD pattern of the USNG, which indicates that there is no regular layer stacking after the reduction of GO because the SnO_2 nanocrystallites can play a part in separating the graphene sheets. SnO_2 nanocrystallites can interact with graphene through charge-transfer interactions, electrostatic binding, or physisorption. By forming of SnO_2 nanocrystallites on the surface of graphene sheets, the stack and aggregation problem of graphene sheets during the reduction process could be avoided, which is beneficial for keeping the excellent physical and chemical properties of graphene.[38] The XRD pattern of USNG matches well with the standard SnO_2 card (JCPDS no. 41-1445), indicating the high purity of the SnO_2 nanocrystallites attached on graphene surfaces. These diffraction peaks are considerably wide, implying ultrasmall size of the SnO_2 nanocrystallites. This result is in agreement with that obtained from TEM observation.

The Raman spectrum is a very useful tool to characterize carbon-based materials. Figure 3b shows the Raman spectra of GO and USNG, which clearly reflect significant structural changes during the process from GO to USNG. The Raman spectra of GO and USNG both contain G band (E_{2g} phonon of C sp^2 atoms) and D band (κ-point phonons of A_{1g} symmetry); however, compared with GO, the D/G intensity ratio of USNG increased obviously (from 0.93 to 1.21). This is a commonly observed phenomenon for chemically converted graphene because the newly formed myriad of sp^2 domains decreased the average size of all the sp^2 domains upon reduction of the GO sheets.[39] This change of Raman spectra from GO to USNG also indicates the successful reduction of GO and the forming of graphene. The location of the G band in carbon-based composites has ever been used to reveal the interaction between carbon and other compounds present.[40,41] Generally, the G band shift in graphene-based composites with nanocrystallites relates to the charge transfer between the graphene and nanocrystallites.[42,43] The Raman spectrum of GO contained a G band at 1604 cm^{-1}, whereas the G band of USNG shifted by 5 cm^{-1} to a lower frequency at 1599 cm^{-1}. Such a shift is due to the charge transfer from the graphene to SnO_2, indicating the strong interaction between graphene and SnO_2.[42] GO yielded an IR spectrum containing peaks at 1729, 1160, 1030, and 872 cm^{-1} corresponding to the vibration of COOH, C−OH, C−O, and O−C═O bonds, respectively, as well as the skeletal vibration of the remaining sp^2 domains at 1587 cm^{-1}. As we can see from the IR spectrum of GO and USNG in Figure 3c, most of the oxygen-containing groups of GO are removed after the hydrothermal reaction. It is well known that the hydrothermal reduction of GO is a very important method to prepare graphene.[44] Moreover, the amines of EDA can react with the oxygen-containing moieties to reduce GO. The IR results further confirm the reduction of GO to graphene. A new strong wide absorption peak centered at 1215 cm^{-1} appears in the IR of USNG, which should be associated with the stretching of C−O in graphene.[45] According to the previous report,[42] the appearance of this new wide peak may also indicate the formation of Sn−O−C bonds in the USNG. X-ray photoelectron spectroscopy (XPS) is a powerful tool to identify the elements' states in bulk material. To confirm the reducing of GO and N-doping of graphene, XPS characterization was carried out. Figure 3d shows the C 1s XPS patterns of GO and USNG. For the GO sample, the spectrum can be deconvoluted into three components, the main peak centered at about 284.8 eV originated from the graphitic sp^2 carbon atoms, and the binding energies located at 286.9 and 288.1 eV are due to carbon atoms connecting with oxygenate groups, C−OH and O−C═O, respectively. Compared with GO, the oxygenate species are substantially removed with the reduction of GO to graphene, which suggests a considerable de-oxygenation process and the successful formation of graphene. For the USNG, a new peak at 286.6 eV corresponding to the C−OSn appears, according to the previous report,[43] which may reflect the forming of Sn−O−C bonds between SnO_2 and graphene. Another new peak at 285.5 eV corresponding to the N−sp^2 C appears, which reflects the bonding status of the C−N bonds, and this new peak is originated from edges or defects of the graphene sheets and the substitution of the N atoms.[46] Figure 3e shows the XPS spectra of the N 1s region for USNG. In the USNG, the N 1s peak has three components, indicating that N atoms are in three different bonding characters doped into the graphene lattice. The peaks at 400.2 and 399.2 eV are attributed to the pyrrolic N (N2) and pyridinic N (N1), respectively.[47] They are ascribed to the N atoms which are located in a π conjugated system and contribute to the π system with two or one p-electrons, respectively.[46] The peak at 401.4 eV corresponds to quaternary N or the "graphitic" N (N3), which are ascribed to the N atoms replacing the inside C atoms of the graphene lattice.[48] On the other hand, the XPS patterns of Sn 3d (Figure 3f) further indicate the existence of SnO_2 nanocrystallites in the USNG. On the basis of XPS analysis discussed above, we can conclude that the reduction of GO to graphene, the deposition of SnO_2 on graphene, and the nitrogen doping of graphene are realized in one step by our method. Because nitrogen has higher electronegativity (3.5) than carbon (3.0) and smaller diameter, the stronger interaction between the formed carbon structure and lithium might be favorable for lithium storage kinetics. The pyridine and pyrrolic N atoms are satisfactorily bonded and may contribute to an enhancement of reversible Li storage capacity.[49] The status of the N-doping can also be unraveled by the elemental mapping images of N in the USNG. The TEM elemental mapping (Figure 4) reveals that the distribution of nitrogen heteroatoms in the plane of graphene is highly homogeneous. The elemental mapping image of C and Sn further confirms that the SnO_2 nanocrystallites are distributed on the graphene uniformly, which is consistent with the TEM observations above.

In this study, we prepared a binder-free, conducting agent-free, current collector-free new type of LIBs by assembling the USNG−GMF bilayered films into the battery directly. In the battery system, the USNG−GMF can function as both electrode materials and separator (Figure 5a). Figure 5b displays the typical charge/discharge curve of the USNG−GMF in the 1st, 2nd, 50th, and 100th cycles. In the first cycle, the discharge capacity dropped rapidly, which can be attributed to the irreversible formation of the amorphous Li_2O matrix and intense surface reactions between the electrolyte solution and the Li−Sn compounds to form a solid electrolyte interface layer (SEI).[50] In the following charge/discharge cycles, Li^+ reversibly reacted with Sn, and the Li_xSn alloys were formed. After the

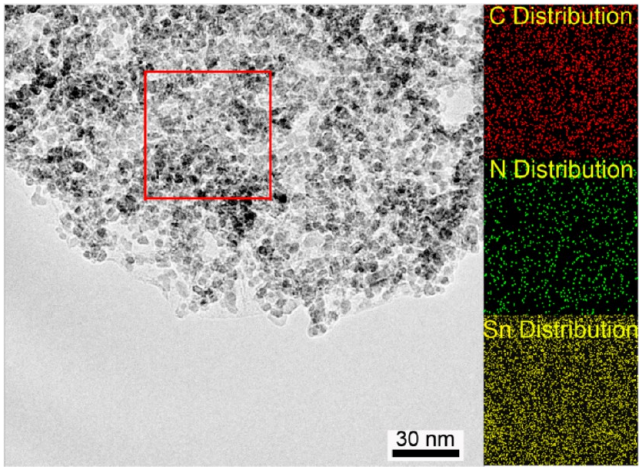

Figure 4. TEM image obtained from the USNG and C-, N-, and Sn-elemental mapping of the square region in the TEM image.

initial capacity fading, the shape of the profiles did not change basically, which indicates the good stability of the USNG. The cycle performances of the USNG−GMF and the single SnO_2 nanocrystallites are shown in Figure 5c. The USNG−GMF exhibited a high reversible discharge capacity of 651 mAh g^{-1} at the second cycle, and from the second cycle, it showed better cycle performance and highly reversible behavior. After 100 cycles, the USNG−GMF can keep about 64.5% retention of the initial reversible capacity, and a discharge capacity of 419.7 mAh g^{-1} still can remain, which is higher than our reported SnO_2/graphene nanocomposite paper and another SnO_2/graphene nanocomposite film for LIBs.[22,23] Compared with the capacity of pure graphene paper (only around 100 mAh g^{-1}), the USNG−GMF exhibited a significantly higher capacity because of the nitrogen doping and the incorporation with higher capacity SnO_2 nanocrystallites. On the other side, the specific capacity of the SnO_2 nanoparticle electrode rapidly decreased from 663 to 163 mAh g^{-1} after 50 cycles. The SnO_2 nanoparticles just hold about 24.6% retention of the reversible capacity due to the severe pulverization of the electrode materials. Compared with the single commercial SnO_2 nanoparticles (50−70 nm) and other reported SnO_2 nanoparticles with diameter about 5 nm, the USNGs exhibit superior discharge capacity and cycling performance.[51] The rate performance of the USNG-GMF is shown in Figure 5d, which was tested at the varied current density from 100 to 3000 mA g^{-1}. The USNG−GMF shows an excellent rate capability. At the higher current densities of 200, 500, and 1000 mA g^{-1}, the USNG−GMF can display specific discharge capacities of 460, 400, and 360 mAh g^{-1}, respectively. Even if the highest current density of 3000 mA g^{-1} was used, the USNG−GMF can still exhibit a high substantial capacity of 285 mAh g^{-1}. It is worth pointing out that, even after 100 cycles, the USNG−GMF still had the ability to display a reversible capacity of 456 mAh g^{-1} when the current density was reversed back to 100 mA g^{-1}. This result demonstrates that 70% of the initial reversible capacity of the USNG is recovered. The result of rate capability clearly indicates that the USNG−GMF could tolerate changed charge/discharge current densities, which is a desirable feature for high power LIB application. The superior LIB performance of the USNG−GMF should be ascribed to the following five unique features of the USNG. First, N-doped graphene can still keep the excellent mechanical properties of pristine graphene. The N-doped graphene sheets covered with the SnO_2 nanocrystallites can form a super flexible coating which not only provides an elastic buffer space to accommodate the volume changes of SnO_2 nanocrystallites during the lithiation/delithiation processes but also successfully prevents the crumbling or cracking of the electrode and the aggregation of the SnO_2 nanocrystallites; thus, a better cycle performance was obtained, whereas the SnO_2 nanoparticle electrode without graphene exhibits a rapid capacity fading due to the large volume change that occurs during the lithiation/delithiation processes, which lead to pulverization and cracking of the electrode.[30] Secondly, compared with the pristine graphene, the doped nitrogen atoms can provide extra lone pair electrons

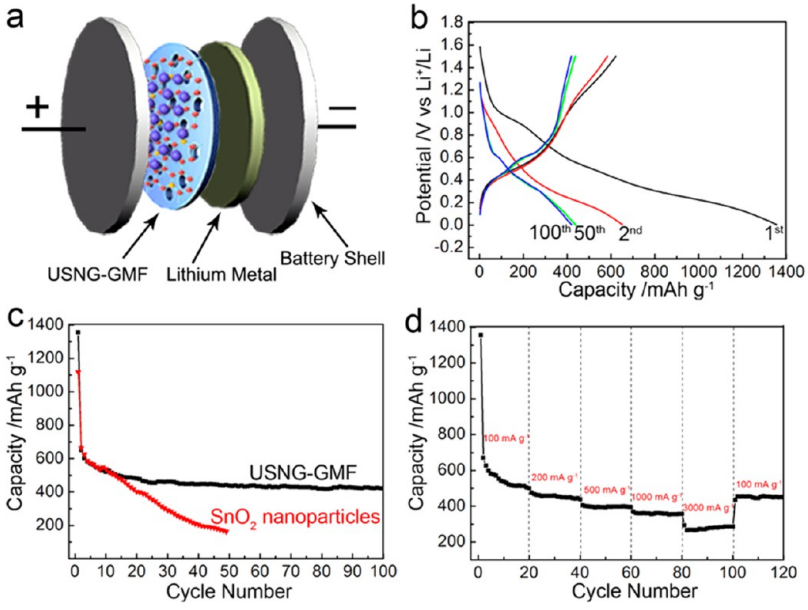

Figure 5. (a) Schematic illustration of the battery electrode assembly. (b) Charge/discharge profile for USNG−GMF paper. (c) The cycle performance of USNG−GMF paper and commercial SnO_2 nanocrystallites. (d) Rate performance of the USNG−GMF paper.

which can efficiently augment the electron density of graphene, and as a result, the N-doped graphene shows more excellent electrical conductivity than the pristine graphene.[29,52] Therefore, the conductivity of the USNG can be significantly improved due to the presence of the excellent conductive N-doped graphene. Moreover, a super conductive network can be built because of the high surface area of the N-doped graphene sheets, which could facilitate the electron transfer during the charge/discharge process. The electronic transport speed in the USNG is faster than the single SnO_2 nanocrystallites. Futhermore, in the USNG, the N-doped graphene nanosheets can act as a continuous conductive path which can effectively reduce the particle−particle interface resistance among the SnO_2 nanocrystallites. The in situ forming of the SnO_2 nanocrystallites and the electrostatic attraction between electron-deficient carbon atoms and electron-rich Sn atoms make the SnO_2 nanocrystallites anchored on the graphene surface firmly, and as a result, the structure stability of the composites was enhanced. The close contact between the ultrasmall SnO_2 nanocrystallites and the super electroconductive N-doped graphene can also weaken the electrical isolation of SnO_2 nanocrystallites during the charge/discharge process. Thirdly, by N-doping, a large number of topological defects are induced to the graphene sheet, and a disordered carbon structure with many surface defects is formed, which make the insertion and extraction processes of Li^+ become much easier, leading to the increase of the reversible capacity. Moreover, the reversible capacity of the pristine graphene can be improved by introducing the pyridinic N atoms.[53] Fourth, the ultrasmall SnO_2 nanocrystallites with good dispersion can both endow the USNG a high surface area to buffer the serious volume expansion/contraction of the SnO_2 and shorten the diffusion route for Li^+ or bring the desirable conductivity to individual SnO_2 nanocrystallites, which are favorable for improving the Li storage performance. Fifth, the good dispersion of ultrasmall SnO_2 nanocrystallites on graphene with large specific surface area can not only provide a large contact area between the electrolyte and the electrode material but also bring a multiple and fast transport pathway for the electrolyte ions. Taking all the above factors together, the special structure of USNG is responsible for the superior LIB performance of the flexible USNG−GMF bilayered film electrode.

4. CONCLUSION

In conclusion, we exploited a green and facile route to synthetize USNG. The method can be used for the preparation of other ultrasmall MO_x nanocrystallites/N-doped graphene nanocomposites for different applications. We explored a novel approach to fabricate flexible electrodes for LIBs by simply depositing USNG on the GMF directly. In our approach, the GMF plays the role of substrate, filter membrane, and separator. Additional separator, current collector, binder, and conducting agents are not needed in the LIB assembly process. The new type of USNG−GMF bilayered film flexible electrode shows high LIB performance. Compared with single SnO_2 nanoparticles, the USNG−GMF shows better cycle performance due to the compositing with excellently electroconductive and flexible N-doped graphene. Compared with pure graphene film, the USNG−GMF exhibits a higher capacity due to the compositing SnO_2 nanoparticles with high capacity and the doping of the nitrogen atom into the graphene lattice. The remarkable LIB performance of USNG−GMF implies that it has great potential for flexible energy storage devices in the future. Furthermore, our new approach for the fabrication of flexible electrodes can be applied to various other electrode materials, which may be useful in flexible or bendable energy storage devices.

AUTHOR INFORMATION

Corresponding Author

*E-mail: guolin@buaa.edu.cn.

Notes

The authors declare no competing financial interest.

ACKNOWLEDGMENTS

This project was supported by the National Natural Science Foundation of China (51272012 & 11079002) as well as by Specialized Research Fund for the Doctoral Program of Higher Education (20111102130006).

REFERENCES

(1) Rogers, J. A.; Someya, T.; Huang, Y. G. *Science* **2010**, *327*, 1603−1607.
(2) Nyholm, L.; Nystrom, G.; Mihranyan, A.; Stromme, M. *Adv. Mater.* **2011**, *23*, 3751−3769.
(3) Tarascon, J. M.; Armand, M. *Nature* **2001**, *414*, 359−367.
(4) Chan, C. K.; Peng, H. L.; Liu, G.; Mcllwrath, G. K.; Zhang, X. F.; Huggin, R. A.; Cui, Y. *Nat. Nanotechnol.* **2008**, *3*, 31−35.
(5) Li, N.; Chen, Z.; Ren, W.; Li, F.; Cheng, H. M. *Proc. Natl. Acad. Sci. U.S.A.* **2012**, *109*, 17360−17365.
(6) Chen, Z.; Zhang, D.; Wang, X.; Jia, X.; Wei, F.; Li, H.; Lu, Y. *Adv. Mater.* **2012**, *24*, 2030−2036.
(7) Liu, F.; Song, S.; Xue, D.; Zhang, H. *Adv. Mater.* **2012**, *24*, 1089−1094.
(8) Jia, X.; Chen, Z.; Suwarnasarn, A.; Rice, L.; Wang, X.; Sohn, H.; Zhang, Q.; Wu, B. M.; Wei, F.; Lu, Y. *Energy Environ. Sci.* **2012**, *5*, 6845−6849.
(9) Jia, X. L.; Yan, C. Z.; Chen, Z.; Wang, R. R.; Zhang, Q.; Guo, L.; Wei, F.; Lu, Y. F. *Chem. Commun.* **2011**, *47*, 9669−9671.
(10) Whittingham, M. S. *Chem. Rev.* **2004**, *104*, 4271−4301.
(11) Gwon, H.; Kim, H. S.; Lee, K. U.; Seo, D. H.; Park, Y. C.; Lee, Y. S.; Ahn, B. T.; Kang, K. *Energy Environ. Sci.* **2011**, *4*, 1277−1283.
(12) Bolotin, K. I.; Sikes, K. J.; Jiang, Z.; Klima, M.; Fudenberg, G.; Hone, J.; Kim, P.; Stormer, H. L. *Solid State Commun.* **2008**, *146*, 351−355.
(13) Lee, C.; Wei, X.; Kysar, J. W.; Hone, J. *Science* **2008**, *321*, 385−388.
(14) Novoselov, K. S.; Geim, A. K.; Morozov, S. V.; Jiang, D.; Zhang, Y.; Dubonos, S. V.; Grigorieva, I. V.; Firsov, A. A. *Science* **2004**, *306*, 666−669.
(15) Geim, A. K. *Science* **2009**, *324*, 1530−1534.
(16) Park, S.; Ruoff, R. S. *Nat. Nanotechnol.* **2009**, *4*, 217−224.
(17) Dikin, D. A.; Stankovich, S.; Zimney, E. J.; Piner, R. D.; Dommett, G. H. B.; Evmenenko, G.; Nguyen, S. T.; Ruoff, R. S. *Nature* **2007**, *448*, 457−460.
(18) Chen, H. Q.; Müller, M. B.; Gilmore, K. J.; Wallace, G. G.; Li, D. *Adv. Mater.* **2008**, *20*, 3557−3561.
(19) Geng, J.; Jung, H. T. *J. Phys. Chem. C* **2010**, *114*, 8227−8234.
(20) Wang, C. Y.; Li, D.; Too, C. O.; Wallace, G. G. *Chem. Mater.* **2009**, *21*, 2604−2606.
(21) Reddy, A. L. M.; Srivastava, A.; Gowda, S. R.; Gullapalli, H.; Dubey, M.; Ajayan, P. M. *ACS Nano* **2010**, *4*, 6337−6342.
(22) Liang, J. F.; Zhao, Y.; Guo, L.; Li, L. D. *ACS Appl. Mater. Interfaces* **2012**, *4*, 5742−5748.
(23) Wang, D. H.; Kou, R.; Choi, D.; Yang, Z. G.; Nie, Z. M.; Li, J.; Saraf, L. V.; Hu, D. H.; Zhang, J. G.; Graff, G. L.; Liu, J.; Pope, M. A.; Aksay, I. A. *ACS Nano* **2010**, *4*, 1587−1595.
(24) Lee, J. K.; Smith, K. B.; Hayner, C. M.; Kung, H. H. *Chem. Commun.* **2010**, *46*, 2025−2027.

(25) Thackeray, M. M.; David, W. I. F.; Bruce, P. G.; Goodenough, J. B. *Mater. Res. Bull.* **1983**, *18*, 461−472.
(26) Idota, Y.; Kubota, T.; Matsufuji, A.; Maekawa, Y.; Miyasaka, T. *Science* **1997**, *276*, 1395−1397.
(27) Yang, J.; Takeda, Y.; Imanishi, N.; Yamamoto, O. *J. Electrochem. Soc.* **1999**, *146*, 4009−4013.
(28) Shi, W.; Rui, X.; Zhu, J.; Yan, Q. *J. Phys. Chem. C* **2012**, *116*, 26685−26693.
(29) Wu, Z. S.; Ren, W. L.; Xu, L.; Li, F.; Cheng, H. M. *ACS Nano* **2011**, *5*, 5463−5471.
(30) Wang, X.; Cao, X. Q.; Bourgeois, L.; Guan, H.; Chen, S. M.; Zhong, Y. T.; Tang, D. M.; Li, H. Q.; Zhai, T. Y.; Li, L.; Bando, Y.; Golberg, D. *Adv. Funct. Mater.* **2012**, *22*, 2682−2690.
(31) Xu, C.; Sun, J.; Gao, L. *Nanoscale* **2012**, *4*, 5425−5430.
(32) Armand, M.; Tatascon, J. M. *Nature* **2008**, *45*, 652−657.
(33) Peng, C.; Chen, B.; Qin, Y.; Yang, S.; Li, C.; Zuo, Y.; Liu, S.; Yang, J. *ACS Nano* **2012**, *6*, 1074−1081.
(34) Kovtyukhova, N. I.; Ollivier, P. J.; Martin, B. R.; Mallouk, T. E.; Chizhik, S. A.; Buzaneva, E. V.; Gorchinskiy, A. D. *Chem. Mater.* **1999**, *11*, 771−778.
(35) Stankovich, S.; Dikin, D. A.; Dommett, G. H. B.; Kohlhaas, K. M.; Zimney, E. Z.; Stach, E. A.; Piner, R. D.; Nguyen, S. T.; Ruoff, R. S. *Nature* **2006**, *442*, 282−286.
(36) Zhong, L. S.; Hu, J. S.; Cui, Z. M.; Wan, L. J.; Song, W. G. *Chem. Mater.* **2007**, *19*, 4557−4562.
(37) Zhu, M. S.; Chen, P. L.; Liu, M. H. *ACS Nano* **2011**, *5*, 4529−4536.
(38) Li, Y. M.; Lv, X. J.; Lu, J.; Li, J. H. *J. Phys. Chem. C* **2010**, *114*, 21770−21774.
(39) Stankovich, S.; Dikin, D. A.; Piner, R. D.; Kohlhaas, K. A.; Kleinhammes, A.; Jia, Y.; Wu, Y.; Nguyen, S. T.; Ruoff, R. S. *Carbon* **2007**, *45*, 1558−1565.
(40) Rao, A. M.; Eklund, P. C.; Bandow, S.; Thess, A.; Smalley, R. E. *Nature* **1997**, *388*, 257−259.
(41) Kitaura, R.; Imazu, N.; Kobayashi, K.; Shinohara, H. *Nano Lett.* **2008**, *8*, 693−699.
(42) Zhou, J. S.; Song, H. H.; Ma, L. L.; Chen, X. H. *RSC Adv.* **2011**, *1*, 782−791.
(43) Zhou, G.; Wang, D. W.; Yin, L. C.; Li, N.; Li, F.; Cheng, H. M. *ACS Nano* **2012**, *6*, 3214−3223.
(44) Zhou, Y.; Bao, Q. L.; Tang, L. A. L.; Zhong, Y. L.; Loh, K. P. *Chem. Mater.* **2009**, *21*, 2950−2956.
(45) Acik, M.; Lee, G.; Mattervi, C.; Chhowalla, M.; Cho, K.; Chabal, Y. J. *Nat. Mater.* **2010**, *9*, 840−845.
(46) Wei, D.; Liu, Y.; Wang, Y.; Zhang, H.; Huang, L.; Yu, G. *Nano Lett.* **2009**, *9*, 1752−1758.
(47) Wang, Y.; Shao, Y. Y.; Matson, D. W.; Li, J. H.; Lin, Y. H. *ACS Nano* **2010**, *4*, 1790−1798.
(48) Casanovas, J.; Ricart, J. M.; Rubio, J.; Illas, F.; Jimenez-Mateos, J. M. *J. Am. Chem. Soc.* **1996**, *118*, 8071−8072.
(49) Ma, X. C.; Wang, E. G. *Appl. Phys. Lett.* **2001**, *78*, 978−980.
(50) Yao, J.; Shen, X. P.; Wang, B.; Liu, H. K.; Wang, G. X. *Electrochem. Commun.* **2009**, *11*, 1849−1852.
(51) Wang, X. Y.; Zhou, X. F.; Yao, K.; Zhang, J. G.; Liu, Z. P. *Carbon* **2011**, *49*, 133−139.
(52) Qiu, Y.; Zhang, X.; Yang, S. *Phys. Chem. Chem. Phys.* **2011**, *13*, 12554−12558.
(53) Wang, H.; Zhang, C.; Liu, Z.; Wang, L.; Han, P.; Xu, H.; Zhang, K.; Dong, S.; Yao, J.; Cui, G. *J. Mater. Chem.* **2011**, *21*, 5430−5434.